

This is the accepted manuscript made available via CHORUS. The article has been published as:

# Exact Model of Vacancy-Mediated Solute Transport in Magnesium

Ravi Agarwal and Dallas R. Trinkle

Phys. Rev. Lett. **118**, 105901 — Published 7 March 2017

DOI: [10.1103/PhysRevLett.118.105901](https://doi.org/10.1103/PhysRevLett.118.105901)

# Exact theory of vacancy-mediated solute transport in magnesium

Ravi Agarwal\* and Dallas R. Trinkle<sup>†</sup>

*Department of Materials Science and Engineering,  
University of Illinois at Urbana-Champaign, Urbana, IL 61801*

(Dated: February 10, 2017)

## Abstract

Most substitutional solutes in solids diffuse via vacancies. However, widely used analytic models for diffusivity make uncontrolled approximations in the relations between atomic jump rates that reduce accuracy. Symmetry analysis of the hexagonal close packed crystal identifies more distinct vacancy transitions than prior models, and a Green function approach computes diffusivity exactly for solutes in magnesium. We find large differences for solute drag of Al, Zn, and rare earth solutes, and improved diffusion activation energies—highlighting the need for exact analytic transport models.

PACS numbers: 66.30.J, 66.30.Fq, 66.10.cg

Diffusion in crystals is a fundamental defect-driven process that controls a variety of different phenomena in materials including ion transport, irradiation-induced degradation of materials, recrystallization, and the formation and growth of precipitates [1]. Developing new alloys requires a precise knowledge of solute transport under various processing conditions. For example, magnesium alloy design focuses on precipitate formation and evolution [2–5], and randomizing the grain texture for improved strain hardening [6–8]. Magnesium alloys may substitute for aluminum and steel in aerospace and automotive industries with their higher specific strengths [9–11]. The growing interest in magnesium has driven experimental [12–19] and computational [20–23] studies of transport coefficients of the common Al and Zn solutes that improve strength and rare earth elements that improve ductility. Transport coefficients are fundamental inputs for models at the length and time scales of microstructure evolution. However, computational modeling of transport coefficients for Mg alloys has used oversimplified models that lead to incorrect predictions, despite using accurate *ab initio* data as inputs [20–23].

In a multicomponent system, diffusivity is described using Onsager transport coefficients  $\underline{L}^{AB}$ , which relates the flux  $\mathbf{J}^A$  of species  $A$  to a chemical potential gradient of species  $B$ :  $\mathbf{J}^A = -\sum_B \underline{L}^{AB} \nabla \mu^B$ . For vacancy-mediated diffusion of a two-component alloy, the transport coefficients for solutes and vacancies are  $\underline{L}^{ss}$ ,  $\underline{L}^{vv}$ , and the off-diagonal coefficient  $\underline{L}^{sv} = \underline{L}^{vs}$ . In the dilute limit, the solute diffusivity  $\underline{D}^s = (k_B T / c_s) \underline{L}^{ss}$  is proportional to the vacancy concentration  $c_v$  and  $c_s$  is the solute concentration. The off-diagonal coefficient can be either positive or negative: the *drag ratio*  $\underline{L}^{sv}(\underline{L}^{ss})^{-1}$  is positive when the flow of vacancies drags solutes in the same direction, and negative when solute flows in the opposite direction to vacancies. The off-diagonal transport coefficient  $\underline{L}^{sv}$  can change sign at the crossover temperature  $T_{\text{cross}}$ . The drag ratio determines how vacancies (e.g. during solidification or irradiation) transport solute to produce non-equilibrium solute segregation, change precipitation rates, or induce the Kirkendall [24] and nano-Kirkendall [25] effects. Anisotropy in the drag ratio leads to unusual flow patterns of solutes [26].

To predict transport coefficients in magnesium alloys, we use a symmetry analysis for automated discovery and cataloging of transitions combined with an analytic, exact Green function (GF) approach which avoids uncontrolled approximations [27, 28]. We identify transitions that are incorrectly treated by the standard 8-frequency model for hexagonal close packed (HCP) crystals [29–31] and even by the recent 13-frequency model [32]. The transition state energy of each transition identified by the symmetry analysis is computed *ab initio*, and directly informs the GF calculation of the transport coefficients. We find significant errors in the drag ratios and solute dif-

fusivities computed by previous models for many technologically important solutes in magnesium. The correct description of the vacancy jump network topology illuminates the atomistic-scale diffusion mechanisms, and the exact calculation of transport coefficients in the dilute limit enables predictive mesoscale modeling of alloys.

Computing transport coefficients requires accurate solute-vacancy binding and transition state energies and entropies from *ab initio*. We use the planewave basis Vienna ab-initio simulation package (VASP) [33–36] with the projector-augmented wave method [37, 38], the PBE generalized gradient approximation exchange-correlation potential [39], and Brillouin zone integration with a Monkhorst-Pack mesh and Methfessel-Paxton smearing [40, 41]. The lanthanide elements are treated with a frozen 4*f*-core, which introduces small errors (below 20 meV) for pure element structures[42], Al-RE convex hulls[43], and is the basis for previous Mg-RE calculations[44]. All convergence criteria are chosen to keep numerical errors below 1 meV (c.f. supplemental material). The climbing-image nudged elastic band method with one intermediate image determines transition state configurations and energies [45], and harmonic transition state theory [46] with the hopping atom approximation [47, 48] computes Arrhenius attempt frequencies (rates). Supplemental Tables SII–SIV show good agreement (deviations below 30 meV) between our calculations and previous calculations [21–23, 44, 49–54] for the vacancy formation energies and solute-vacancy binding, where available. Supplemental Tables SV and SVI compare the limited set of transition state energies required in 8-frequency model from previous work [20–23] with our complete dataset [55].

An exact GF approach [27] computes the transport coefficients for dilute solutes and vacancies from our *ab initio* data. The hexagonal lattice ensures that the transport coefficients are diagonal but anisotropic with different basal plane and *c*-axis values. The symmetry operations in the HCP space group  $P6_3/mmc$  [56] determine equivalent solute-vacancy complex states and equivalent transition states. We identify transition states by the initial and final states, and consider two transition states equivalent when a single space group operation can simultaneously transform the initial and final states for one transition state into the other. From the solute-vacancy probabilities and transition rates, we treat the correlated random walk [57–59] using the vacancy Green function: first computed in the absence of the solute, and then corrected for the presence of solute using the Dyson equation. We compute the Green function without solute in reciprocal space, and the Dyson equation correction in real space, taking advantage of computer-determined symmetry[28]. This approach is a generalization of the matrix method [60–62]. For the dilute limit with a single

solute and single vacancy, the calculated transport coefficients are exact [27].

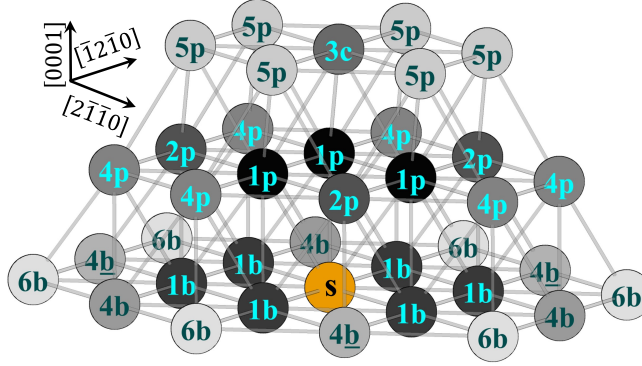


FIG. 1. Possible vacancy-solute complexes out to sixth nearest-neighbors in a HCP crystal. Complexes are identified by the position of the vacancy relative to the solute (orange “s”). There are nine unique complexes, corresponding to 56 configurations after applying symmetry operations; vacancy positions below the solute are not shown. Complexes are labeled by the shell distance between solute and vacancy (lighter colors correspond to larger separation), and with “b” (basal), “p” (prismatic), and “c” (c-axis). Vacancy neighbor distance is insufficient to identify symmetry unique complexes: the 1b and 1p complexes, and 4b, 4 $\bar{b}$  and 4p complexes each have different binding energies.

In the HCP crystal, there are two unique first nearest-neighbor vacancy-solute complexes and seven complex configurations that are one transition away; Figure 1 shows these complexes out to 6b. A solute has six first neighbors in the same basal plane (1b sites), and six in the neighboring basal planes (1p sites). We expect these complexes to have the strongest solute-vacancy binding energy. The solute-vacancy binding also changes the transition states for vacancy motion, leading to various types of jumps: exchange with the solute, jumps between first neighbor sites, and jumps away from the solute. The latter generates seven complex configurations; in the 8-frequency model, these seven complexes and all further ones are assumed to have no vacancy-solute binding.

Figure 2 enumerates the 15 unique transitions for first neighbor vacancy-solute complexes. Away from a solute, the vacancy can jump in a basal or pyramidal direction. The symmetry unique transitions for complexes includes two types of vacancy-solute exchanges, four transition states between first neighbor complexes, and another nine transitions from the two first neighbor to the seven different “outer” complexes, which correspond to dissociation. In contrast, the standard 8-frequency model [29–31] assumes that the two different 1b to 1b transitions, that we call 1b-1b and  $\underline{1b-1b}$ , have equal transition rates. Moreover, it assumes that all of the dissociation transition

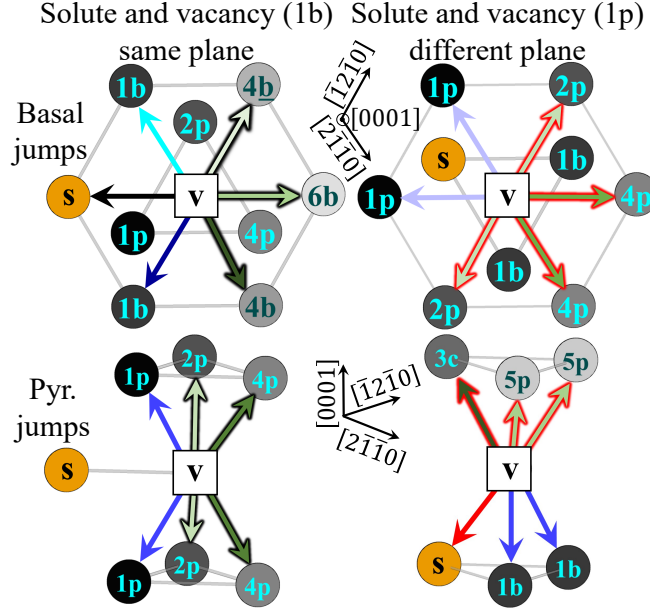


FIG. 2. Vacancy (v) jumps in an HCP crystal from 1b and 1p complexes, divided into basal and pyramidal jumps. The 24 jumps correspond to two solute-vacancy exchanges (black and red arrows), eight vacancy reorientations around the solute (arrows in blue), and 14 solute-vacancy complex dissociations (arrows in green with outline in black from 1b configuration and outline in red from 1p configuration). In particular, two reorientation jumps of the 1b complex that the 8-frequency model treats as equal are not related by symmetry: 1b-1b (cyan) and 1b-1b (dark blue) jumps in the top-left figure. The symmetry inequivalence can be identified by the different Mg atoms neighboring the transition states: Mg at 2p for 1b-1b and 1p sites for 1b-1b.

rates can be reduced to two: one out of the 1b site, one out of the 1p site [63]. However, we find that Zn, Al and rare earth elements have markedly different migration barriers for 1b-1b and 1b-1b jumps and have different dissociation barriers (c.f. supplemental Tables SV and SVI). Recently, Nandipati *et al.* also found the distinction between 1b-1b and 1b-1b jump using self-learning kinetic Monte Carlo [64]. As previous computational studies [20–23] relied on the 8-frequency framework to model diffusion and identify which transition states to compute, these uncontrolled approximations can cause significant quantitative and qualitative errors in transport coefficients. Note that even the recent 13-frequency model of Allnatt *et al.* also assumes that 1b-1b and 1b-1b jumps are equivalent [32].

Solute drag requires a “ring” network around the solute [65, 66], so that the vacancy-solute complex can reorient and produce long-range diffusion; Figure 3 shows the three minimal rings

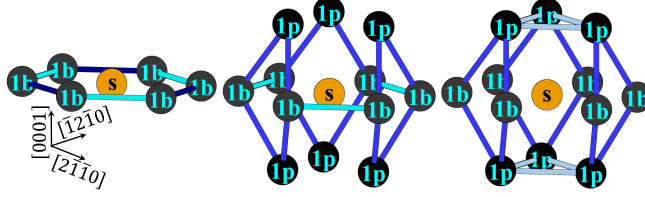


FIG. 3. Minimal networks of reorientation jumps for 1b and 1p complexes. (Left) Network in the basal plane requiring only 1b-1b and  $\underline{1b-1b}$  jumps. (Middle) Network of 1p-1b and 1b-1b jumps. (Right) Network of 1p-1b and 1p-1p jumps. The other three pairings of jumps do not form closed ring networks, and are not shown. Ring networks are necessary for a complex to diffuse as a unit, leading to positive drag ratios.

with the necessary pairs of jumps. For a complex to diffuse as a unit, a vacancy-solute exchange must be followed by vacancy reorientation jumps around the solute; otherwise, exchanges keep the complex in place. To make a ring network in HCP requires at least two “fast” jump rates. However, the network topology is such that out of the six possible pairs of jumps, only three are able to produce reorientation rings. Two pairs of transitions—combining 1p-1p with 1b-1b or  $\underline{1b-1b}$ —clearly lack sufficient connectivity to reorient a complex in arbitrary ways. It is surprising that combining 1p-1b jumps with  $\underline{1b-1b}$  jumps fails to produce reorientation while combining 1p-1b jumps with 1b-1b jumps does; this asymmetric jump network topology for 1b-1b and  $\underline{1b-1b}$  has significant impact on the drag ratios.

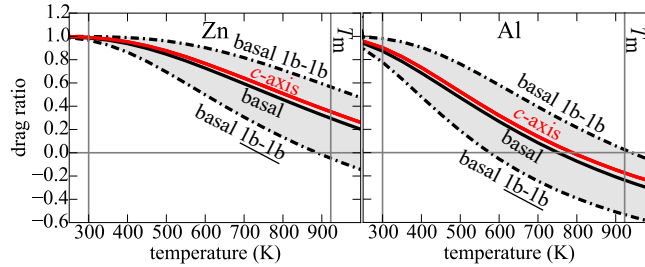


FIG. 4. Effect of 1b-1b and  $\underline{1b-1b}$  asymmetry on the drag ratio  $\underline{L}^{sv}(\underline{L}^{ss})^{-1}$  of Zn and Al. Both the 8-frequency and 13-frequency framework assumes  $\omega_{1b-1b}$  and  $\omega_{\underline{1b-1b}}$  rates to be equal; this gives different basal drag ratios if  $\omega_{1b-1b}$  or  $\omega_{\underline{1b-1b}}$  is used for both rates (dotted-dashed lines), but does not affect *c*-axis diffusion. The GF method treats the nonequivalent transitions when computing the correct basal drag ratio (solid lines). The 8-frequency and 13-frequency framework introduce additional approximations which affect drag ratios and crossover temperatures, and incorrectly predict large anisotropy in drag ratios.

Figure 4 shows the errors from using the 8-frequency and 13-frequency framework to compute

the drag ratios of Zn and Al in Mg. For Zn and Al, the reorientation rates in the ring network are fast and there is a significant difference in the 1b-1b and  $\underline{1b-1b}$  migration barriers, with lower 1b-1b migration barriers (by 0.22 eV for Zn and by 0.14 eV for Al). The 8-frequency and 13-frequency frameworks enforce  $\omega_{1b-1b} = \omega_{\underline{1b-1b}}$ , which produces significant errors. The faster  $\omega_{1b-1b}$  rate gives a higher drag ratio, while the slower  $\omega_{\underline{1b-1b}}$  rate gives a lower drag ratio—neither of which agrees with the exact GF result. The correct behavior is difficult to reproduce with either framework, as the  $\omega_{1b-1p}$  rate is slower than the  $\omega_{1b-1b}$ , but faster than  $\omega_{\underline{1b-1b}}$ : the first two ring networks in Fig. 3 contribute significantly to drag, but choosing a single value of  $\omega_{1b-1b} = \omega_{\underline{1b-1b}}$  affects the two rings differently. Moreover, all prior DFT calculations[20–23] only computed one of the two barriers, as the 8-frequency model does not suggest that there are two distinct jumps to consider. This error does not impact the *c*-axis drag ratio, while a small change in solute diffusivity  $D^s$  is observed. It does explain the discrepancies in the migration barrier reported by different authors, as each selected either 1b-1b or  $\underline{1b-1b}$ .

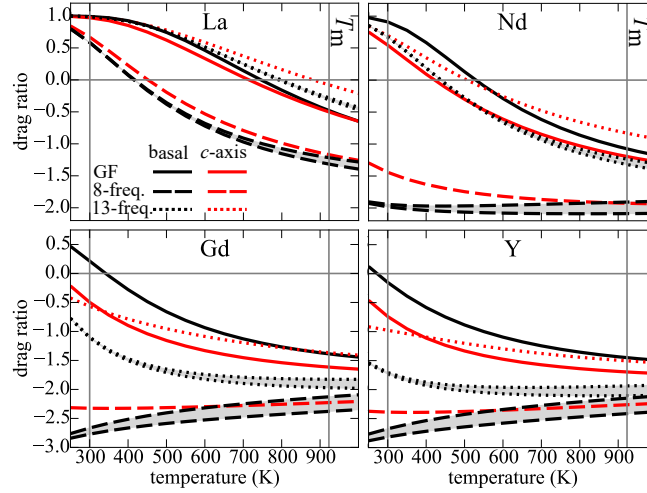


FIG. 5. Effect of dissociation rates on drag ratio  $\underline{L}^{sv}(\underline{L}^{ss})^{-1}$  of La, Nd, Gd and Y. The 8-frequency framework (dashed lines) and 13-frequency framework (dotted lines) reduces the nine distinct dissociation rates to two and four, which causes errors in both basal and *c*-axis drag ratios. The 13-frequency framework improves over the 8-frequency model but still has errors in drag ratios for Gd and Y, and predicts incorrect anisotropy. Filled regions in grey with the bounds for basal drag from 8- and 13-frequency model captures the approximation of  $\omega_{1b-1b}$  or  $\omega_{\underline{1b-1b}}$  rates. Table I includes additional data on crossover temperatures.

Figure 5 shows the drag ratio is also affected by different dissociation rates for La, Nd, Gd and Y in Mg. For these solutes, association and dissociation rates are faster than reorientation,

TABLE I. Activation energies of diffusion  $Q$  and crossover temperatures  $T_{\text{cross}}$  computed with the GF method, 8-frequency, 13-frequency model and available experimental data in the basal plane and along the  $c$ -axis. All values are reported as basal| $c$ -axis, while Nd, Ce, and La experiments correspond to polycrystals. Activation energies using GF method are lower by  $\sim 0.1$  eV compared to the 8-frequency model for Nd, Ce, La and Gd; this improves the agreement with experiment for all except Ce. There are significant changes to crossover temperatures, the 8-frequency calculation doesn't predict drag for Gd and Y, and the 13-frequency predictions are off by more than 100 K for Nd, Ce, La and Ca along  $c$ -axis and for Gd and Y in basal plane.

Solute	$Q$ (eV)				$T_{\text{cross}}$ (K)		
	8-freq.	13-freq.	GF	Experiment	8-freq.	13-freq.	GF
Nd	1.18 1.20	1.12 1.12	1.08 1.13	1.16 [18]	< 100	438 507	529 422
Ce	1.14 1.15	1.07 1.07	1.03 1.09	1.82 [12]	252 287	635 721	648 589
La	1.10 1.11	1.02 1.03	1.00 1.04	1.06 [12]	415 452	795 881	746 714
Gd	1.24 1.26	1.19 1.18	1.16 1.17	0.82 0.85 [16]	—	175 155	341 218
Y	1.25 1.27	1.21 1.21	1.20 1.21	1.01 1.02 [16]	—	106  < 100	271 190
Ca	1.12 1.14	1.09 1.09	1.08 1.11	1.07 [19]	309 343	538 598	538 501

and positive drag ratio results from an “outer” vacancy ring network around the solute—similar to the behavior in BCC and FCC lattices [65, 66]. There are three outer ring networks which can contribute to drag: 1b-4b and 1b-4 $\bar{b}$ ; 1p-2p and 1b-2p; and 1b-4p, 1p-4p and 1p-3c. The 8-frequency and 13-frequency frameworks reduces all nine of the different association/dissociation transition states to two: 1b- $\infty$  and 1p- $\infty$ , or four: basal and pyramidal type jump of 1b- $\infty$  and 1p- $\infty$ , where “ $\infty$ ” is any non-first neighbor complex. We compare our full calculation to the 8-frequency (using 1b-6b and 1p-5p) and 13-frequency (using 1b-6b, 1b-4p, 1p-4p and 1p-5p) models. These dissociation jumps in the 8-frequency model for La, Nd, Gd and Y are the slowest dissociation rates; hence, the 8-frequency model underpredicts the vacancy residency time in the outer ring network. This impacts the drag ratio, where the 8-frequency framework predicts no drag for Nd, Gd and Y, and reduced drag for La. The improved 13-frequency model still has error in drag for Gd and Y due to the incorrect contribution from 1b-4p, 1p-4p and 1p-3c ring as well as from  $\omega_{1b-1b}=\omega_{1\bar{b}-1b}$  rate assumption.

Table I shows improvement in solute diffusivity predictions for rare-earth and Ca solutes com-

pared with available experimental data. The assumptions made in the 8-frequency framework lead to inaccurate calculation of correlation factors and activation energies. Ghate [30] assumed a constant value for the vacancy escape factor  $F = 0.736$  in the 8-frequency model for solute correlation factors ( $f_{A,z}$ ,  $f_{A,b}$ , and  $f_{B,x}$  in Eq. (12–16) of [30]) affecting the probability for a vacancy return after dissociation. Manning showed that in FCC crystals,  $F$  depends on the ratio of vacancy solute association rate and vacancy migration rates in bulk, and hence depends on temperature [57]. The GF approach correctly computes  $F$  and its dependence on all of the transition rates near the solute [27]. The errors from the 8-frequency or 13-frequency model are solute dependent, and are larger for solutes with faster dissociation and exchange rates. Hence, rare earth solutes have activation energies for diffusion that are lowered by 0.05–0.1 eV, improving agreement with experimental measurements for all except Ce. The crossover temperature shows significant error when computed using the 8-frequency framework, with some improvement as some approximations are eliminated in the 13-frequency framework. The remaining disagreement with experiment suggests new experimental studies, and a reexamination of the appropriateness of the frozen  $4f$ -core approximation for lanthanides, especially for Ce.

A full symmetry analysis of solute-vacancy complex states and transition states combined with an exact Green function methodology removes uncontrolled approximations from transport modeling, and reveals significant errors in previous calculations. Identifying the symmetry unique transitions in the vacancy jump network elucidates the fundamental mechanisms responsible for solute drag and provide quantitative values for transport coefficients. Our analysis has application to diffusivity calculations in other crystalline systems—especially where the solute-vacancy binding extends beyond first neighbors. Removing uncontrolled approximations from the prediction of transport coefficients is important for the validation of *ab initio* methods, from which we can identify possible systematic errors in the computation of atomic-scale diffusion mechanisms. Our results also show the importance of proper symmetry analysis to identify atomic scale transport mechanisms, even for well-studied crystalline systems like HCP.

This research was supported by the U.S. Office of Naval Research under the grant N000141210752 and the National Science Foundation Award 1411106. This work used the Extreme Science and Engineering Discovery Environment (XSEDE) [67], which is supported by National Science Foundation grant number ACI-1053575 at the Texas Advanced Computing Center. Figures 1, 2 and 3 are generated using the Jmol package [68]. The authors thank Abhinav Jain, Thomas Schuler, and Pascal Bellon for helpful conversations and suggestions for the manuscript.

---

\* ragarwl4@illinois.edu

† dtrinkle@illinois.edu

- [1] R. W. Balluffi, S. M. Allen, and W. C. Carter, *Kinetics of Materials* (John Wiley & Sons, Inc., 2005).
- [2] A. Luo, *International Materials Reviews* **49**, 13 (2004).
- [3] C. L. Mendis, C. J. Bettles, M. A. Gibson, S. Gorsse, and C. R. Hutchinson, *Philosophical Magazine Letters* **86**, 443 (2006).
- [4] C. Mendis, K. Oh-ishi, and K. Hono, *Scripta Materialia* **57**, 485 (2007).
- [5] J.-F. Nie, *Metallurgical and Materials Transactions A* **43**, 3891 (2012).
- [6] J. Bohlen, M. R. Nürnberg, J. W. Senn, D. Letzig, and S. R. Agnew, *Acta Materialia* **55**, 2101 (2007).
- [7] T. Laser, C. Hartig, M. Nürnberg, D. Letzig, and R. Bormann, *Acta Materialia* **56**, 2791 (2008).
- [8] N. Stanford, *Materials Science and Engineering: A* **527**, 2669 (2010).
- [9] H. E. Friedrich and B. L. Mordike, *Magnesium Technology*, 1st ed. (Springer-Verlag Berlin Heidelberg, 2006).
- [10] T. M. Pollock, *Science* **328**, 986 (2010).
- [11] W. Joost, *JOM* **64**, 1032 (2012).
- [12] K. Lal and V. Levy, *Comptes Rendus de l'Académie des Sciences Series C* **262**, 107 (1966).
- [13] J. Čermák and I. Stloukal, *physica status solidi (a)* **203**, 2386 (2006).
- [14] S. Brennan, A. P. Warren, K. R. Coffey, N. Kulkarni, P. Todd, M. Kilmov, and Y. Sohn, *Journal of Phase Equilibria and Diffusion* **33**, 121 (2012).
- [15] S. K. Das, Y.-M. Kim, T. K. Ha, and I.-H. Jung, *Calphad* **42**, 51 (2013).
- [16] S. K. Das, Y.-B. Kang, T. Ha, and I.-H. Jung, *Acta Materialia* **71**, 164 (2014).
- [17] C. Kammerer, N. Kulkarni, R. Warmack, and Y. Sohn, *Journal of Alloys and Compounds* **617**, 968 (2014).
- [18] M. Paliwal, S. K. Das, J. Kim, and I.-H. Jung, *Scripta Materialia* **108**, 11 (2015).
- [19] W. Zhong and J.-C. Zhao, *Scripta mater.* **127**, 92 (2017).
- [20] S. Ganeshan, L. G. Hector, Jr., and Z.-K. Liu, *Acta Materialia* **59**, 3214 (2011).
- [21] L. Huber, I. Elfimov, J. Rottler, and M. Militzer, *Phys. Rev. B* **85**, 144301 (2012).
- [22] B.-C. Zhou, S.-L. Shang, Y. Wang, and Z.-K. Liu, *Acta Materialia* **103**, 573 (2016).
- [23] H. Wu, T. Mayeshiba, and D. Morgan, *Scientific Data* **3**, 160054 (2016).

- [24] A. Smigelskas and E. Kirkendall, Trans. AIME **171**, 130 (1947).
- [25] Y. Yin, R. M. Rioux, C. K. Erdonmez, S. Hughes, G. A. Somorjai, and A. P. Alivisatos, Science **304**, 711 (2004).
- [26] T. Garnier, V. R. Manga, D. R. Trinkle, M. Nastar, and P. Bellon, Phys. Rev. B **88**, 134108 (2013).
- [27] D. R. Trinkle, “Automatic numerical evaluation of vacancy-mediated transport for arbitrary crystals: Onsager coefficients in the dilute limit using a Green function approach,” (2016), (under review, J. Math. Phys.), arXiv:1608.01252.
- [28] D. R. Trinkle, “ONSAGER,” <http://dallastrinkle.github.io/Onsager> (2016).
- [29] H. B. Huntington and P. B. Ghate, Phys. Rev. Lett. **8**, 421 (1962).
- [30] P. B. Ghate, Phys. Rev. **133**, A1167 (1964).
- [31] A. P. Batra, Phys. Rev. **159**, 487 (1967).
- [32] A. Allnatt, I. Belova, and G. Murch, Philos. Mag. **94**, 2487 (2014).
- [33] G. Kresse and J. Hafner, Phys. Rev. B **47**, 558 (1993).
- [34] G. Kresse and J. Hafner, Phys. Rev. B **49**, 14251 (1994).
- [35] G. Kresse and J. Furthmüller, Computational Materials Science **6**, 15 (1996).
- [36] G. Kresse and J. Furthmüller, Phys. Rev. B **54**, 11169 (1996).
- [37] P. E. Blöchl, Phys. Rev. B **50**, 17953 (1994).
- [38] G. Kresse and D. Joubert, Phys. Rev. B **59**, 1758 (1999).
- [39] J. P. Perdew, K. Burke, and M. Ernzerhof, Phys. Rev. Lett. **77**, 3865 (1996).
- [40] H. J. Monkhorst and J. D. Pack, Phys. Rev. B **13**, 5188 (1976).
- [41] M. Methfessel and A. T. Paxton, Phys. Rev. B **40**, 3616 (1989).
- [42] W. M. Temmerman, L. Petit, A. Svane, Z. Szotek, M. Lüders, P. Strange, J. Staunton, I. D. Hughes, and B. L. Gyorffy, in *Chapter 241 The Dual, Localized or BandLike, Character of the 4f-States*, Handbook on the Physics and Chemistry of Rare Earths, Vol. 39 (Elsevier, 2009) pp. 1–112.
- [43] M. C. Gao, A. D. Rollett, and M. Widom, Phys. Rev. B **75**, 174120 (2007).
- [44] J. E. Saal and C. Wolverton, Acta Materialia **60**, 5151 (2012).
- [45] G. Henkelman, B. P. Uberuaga, and H. Jónsson, The Journal of Chemical Physics **113**, 9901 (2000).
- [46] G. H. Vineyard, Journal of Physics and Chemistry of Solids **3**, 121 (1957).
- [47] H. H. Wu and D. R. Trinkle, Phys. Rev. Lett. **107**, 045504 (2011).
- [48] R. Agarwal and D. R. Trinkle, Phys. Rev. B **94**, 054106 (2016).
- [49] H. Krimmel and M. Fähnle, Phys. Rev. B **62**, 5489 (2000).

- [50] N. Chetty, M. Weinert, T. S. Rahman, and J. W. Davenport, Phys. Rev. B **52**, 6313 (1995).
- [51] S. Ganeshan, L. G. Hector, Jr., and Z.-K. Liu, Computational Materials Science **50**, 301 (2010).
- [52] D. Shin and C. Wolverton, Acta Materialia **58**, 531 (2010).
- [53] T. Angsten, T. Mayeshiba, H. Wu, and D. Morgan, New Journal of Physics **16**, 015018 (2014).
- [54] S.-L. Shang, B.-C. Zhou, W. Y. Wang, A. J. Ross, X. L. Liu, Y.-J. Hu, H.-Z. Fang, Y. Wang, and Z.-K. Liu, Acta Materialia **109**, 128 (2016).
- [55] See Supplemental Material at <http://link.aps.org/supplemental/10.1103/PhysRevLett.XXX.YYYYYY> for convergence criteria, PAW choice (supplemental Table SI), a full list of all computational data, comparisons with other computational studies, which also includes Refs. [69–74].
- [56] T. Hahn, ed., *International Tables for Crystallography*, 4th ed., Vol. A (Dordrecht: Kluwer Academic, 1996).
- [57] J. R. Manning, Phys. Rev. **128**, 2169 (1962).
- [58] J. R. Manning, *Diffusion Kinetics for Atoms in Crystals* (Princeton: van Nostrand, 1968).
- [59] A. R. Allnatt and A. B. Lidiard, “Atomic transport in solids,” (Cambridge University Press, Cambridge, 1993) Chap. 5, pp. 202–203.
- [60] E. W. Montroll and G. H. Weiss, J. Math. Phys. **6**, 167 (1965).
- [61] M. Koiwa and S. Ishioka, Philos. Mag. A **47**, 927 (1983).
- [62] J. L. Bocquet, Philos. Mag. **94**, 3603 (2014).
- [63] The eight frequencies (rates) are:  $\omega_{1b-1b} = \omega_{\underline{1b-1b}}$ ,  $\omega_{1p-1p}$ ,  $\omega_{1p-1b}$ ,  $\omega_{1b-1p}$ ,  $\omega_{1b-s}$ ,  $\omega_{1p-s}$ ,  $\omega_{1b-\infty}$ ,  $\omega_{1p-\infty}$ ,  $\omega_{\infty-1b}$ , and  $\omega_{\infty-1p}$ .
- [64] G. Nandipati, N. Govind, A. Andersen, and A. Rohatgi, Journal of Physics: Condensed Matter **28**, 155001 (2016).
- [65] T. Garnier, M. Nastar, P. Bellon, and D. R. Trinkle, Phys. Rev. B **88**, 134201 (2013).
- [66] T. Garnier, D. R. Trinkle, M. Nastar, and P. Bellon, Phys. Rev. B **89**, 144202 (2014).
- [67] J. Towns, T. Cockerill, M. Dahan, I. Foster, K. Gaither, A. Grimshaw, V. Hazlewood, S. Lathrop, D. Lifka, G. Peterson, R. Roskies, J. Scott, and N. Wilkins-Diehr, Computing in Science Engineering **16**, 62 (2014).
- [68] Jmol: An open-source Java viewer for chemical structures in 3D.
- [69] C. Janot, D. Malléjac, and B. George, Phys. Rev. B **2**, 3088 (1970).
- [70] C. Mairy, J. Hillairet, and D. Schumacher, Acta Metallurgica **15**, 1258 (1967).
- [71] P. Tzanetakis, J. Hillairet, and G. Revel, Physica Status Solidi (B) Basic Research **75**, 433 (1976).

- [72] J. Combronde and G. Brebec, *Acta Metallurgica* **19**, 1393 (1971).
- [73] J. Delaplace, J. Hillairet, J. C. Nicoud, D. Schumacher, and G. Vogl, *physica status solidi (b)* **30**, 119 (1968).
- [74] B.-C. Zhou, S.-L. Shang, Y. Wang, and Z.-K. Liu, *Data in Brief* **5**, 900 (2015).